FSI Analysis of Solitary Wave Interacting with Horizontal Flexible Plate by MPS-FEM Method

Chengping Rao, Youlin Zhang, Decheng Wan[*]
Collaborative Innovation Center for Advanced Ship and Deep-Sea Exploration, State Key Laboratory of Ocean Engineering,
School of Naval Architecture, Ocean and Civil Engineering, Shanghai Jiao Tong University, Shanghai, China
[*] Corresponding author

ABSTRACT

That the solitary wave impacting onto the horizontal plate above the surface is investigated numerically using Moving Particle Semi-Implicit and finite element coupled method (MPS-FEM) in this paper. The wave-induced force and pressure distribution on the bottom of the plate are the major concerns in this research. Case of the rigid plate in three-dimensional situations is initially considered. The comparisons between the calculated vertical and horizontal force and the available experimental results show fair agreement, which indicate that the solver can successfully predict the wave-induced forces. The simulation of two-dimensional solitary wave impacting onto flexible plate is finally conducted. Results from cases of the flexible and the rigid plate are compared to investigate the effects of flexibility on the wave-plate interaction.

KEY WORDS: Moving Particle Semi-implicit (MPS); Finite element method (FEM); Fluid-structure interaction (FSI); Solitary wave; MLParticle-SJTU solver

INTRODUCTION

The model of wave interacting with horizontal plate is commonly observed in the offshore and coastal engineering. For example, a very large floating structure (VLFS) with its horizontal size much greater than the vertical size is usually treated as thin plate floating in the ocean. While encountering severe wave, it could produce considerable deformation which will exert a great influence on the flow field nearby, making the problem more complex. Apart from VLFS, offshore drilling platform, coastal bridge and wave-breaker are among the structures suffering from the impact of the wave. To ensure the safety of these structures, the fluid-structure interaction (FSI) analysis is sometimes indispensable.

The interaction between wave and plate is an issue widely investigated by the researchers. In the early times, scholars such as Kaplan et al.

(1995) adopted an empirical method to study the wave-plate interaction problem. The wave-induced forces are decomposed into the components of slamming force, drag force, inertia force and buoyancy force, which are determined according to the results of physical model tests. Allsop et al. (2006) tried to divide the forces into the components of slowly varying load and the short-duration impact load in order to analyze the jetties/piers exposed to large waves. Some scholars also managed to calculate the time-dependent loads on a plate with numerical methods. Seiffert et al. (2014) obtained the wave-induced force on a flat plate under the solitary wave with various amplitudes, water depths and vertical positions using the open source CFD software - OpenFOAM. Hayatdavoodi et al. (2015) adopted the Green-Naghdi theory to investigate the interaction between solitary and cnoidal waves and submerged horizontal plate. The nonlinear forces and overturning moment are obtained using the Level I Green-Naghdi nonlinear-wave equations.

However, the above researches ignore the flexibility of the plate. Just as mentioned, taking the flexibility of structure into consideration is of interests since the deformation could harm significantly the safety of structures. The existent FSI analysis for this problem is much fewer. Faltinsen et al. (1995) studied the wave impact on a horizontal elastic plate theoretically with the help of hydroelasticity theory and extension of the asymptotic method. Structural stress caused by slamming is mainly focused. Under the small-amplitude wave hypothesis and the potential flow theory, Meng and Lu (2017) investigated the wave-induced responses of a semi-immersed rigid body connected with an elastic plate, which is assumed to be the simplified model of VLFS. Nelli et al. (2016) conducted the experiment of a free-floating elastic plate under regular wave to investigate the effects of deformation on wave reflection and transmission.

In recent years, numerical approaches, which can provide with comprehensive information and consume much less resource than the experiment, become advantageous in the analysis of FSI problems. Liu and Sakai (2002) investigated the hydroelastic responses of a 2D flexible plate exposed to waves using BEM for fluid and FEM for structure. Liao and Hu (2012) adopted FDM-FEM coupled method to

study the interaction between surface flow and thin elastic plate. The above numerical approaches are two representative mesh-based methods. Despite the effectiveness, these mesh-based methods may suffer from the difficulties such as the adjustment or regeneration of mesh so as to coordinate the interface between fluid and structure domain. Some newly emerged meshfree (or meshless) methods can exactly overcome the difficulties brought about by the mesh. These meshfree methods display fair adaptation to the problems of large deformation and intense surface because there is no requirement for treatments of mesh or free surface. The Smoothed Particle Hydrodynamics (SPH) proposed by Lucy (1977), Monaghan and Gingold (1977), became one of the most popular meshfree methods adopted in hydrodynamics after multiple modifications (Khayyer et al. 2017; Lind et al. 2012). And some scholars managed to combine it with other methods to solve the FSI problems. FEM has been incorporated into meshfree particle methods to solve FSI problems. Although the SPH-FEM model was first proposed by Attaway et al. (1994) to investigate the structure-structure interaction, it was subsequently applied into FSI problems (Antoci et al. 2007; Fourey et al. 2010; Yang et al. 2012; Long et al. 2016). The Moving Particle Semi-implicit (MPS) is another typical particle-based meshfree method. It is first proposed by Koshizuka and Oka (1996) to solve the hydrodynamics problems. It was subsequently applied into the field of ocean engineering (Gotoh and Khayyer. 2016). Different from the traditional SPH method, the pressure of the particle is obtained by solving the Poisson's pressure equation (PPE) in the MPS method. Thus the obtained pressure field through MPS method is relatively smoother. A great deal of research concerning FSI has been conducted in the basis of the MPS method. Sun et al. (2016) proposed MPS-modal superposition method in which the elastic deformation of structure is computed through a mode superposition formulation. Actually, more scholars chose to adopt MPS-FEM model in order to address complicated FSI problem. Lee et al. (2007) successfully simulated the interaction between dam-break and sloshing flow through the coupled MPS-FEM method. Some other research performing the MPS-FEM model (Mitsume et al. 2014; Hwang et al. 2014; Hwang et al. 2016; Zhang et al. 2016a) also displayed fair agreement with available experimental results.

The primary objective of this paper is to investigate numerically the wave-plate interaction through the MPS-FEM coupled method. The Moving Particle Semi-Implicit (MPS) method is used to simulate the fluid domain while the finite element method (FEM) is employed to calculate the structural motion. The theories and coupling strategy are briefly introduced. The simulation of three-dimensional wave-plate interaction is conducted whose results are then compared with the available experimental results. Then we simulate the solitary wave impacting onto the horizontal flexible plate. The case of flexible plate is compared with that of rigid to investigate the effects of flexibility on the wave-induced force and pressure distribution on the bottom of plate.

NUMERICAL METHOD

In this study, the MPS-FEM coupled method is adopted to investigate the wave-plate interaction problem. The improved MPS method is used to simulate the fluid motion while the FEM is employed to calculate the structural domain. The theory for the MPS and FEM have been presented with details in our previous papers (Zhang and Wan, 2012; Zhang et al., 2014; Tang et al., 2015; Tang et al., 2016; Zhang et al., 2016b; Zhang and Wan. 2017). Thus are introduced briefly in this section.

MPS formulas

The governing equations for viscous incompressible fluid contain continuity equation and N-S equation:

$$\nabla \cdot \boldsymbol{V} = 0 \tag{1}$$

$$\frac{D\boldsymbol{V}}{Dt} = -\frac{1}{\rho}\nabla P + \nu\nabla^2\boldsymbol{V} + \boldsymbol{g} \tag{2}$$

where ρ is fluid density, P is pressure, $\boldsymbol{V}$ is velocity vector, $\boldsymbol{g}$ is gravitational acceleration, ν is kinematic viscosity coefficient. The kernel function in present paper is

$$W(r) = \begin{cases} \dfrac{r_e}{0.85r + 0.15r_e} - 1 & 0 \leq r < r_e \\ 0 & r_e \leq r \end{cases} \tag{3}$$

where $r = |r_j - r_i|$ is the distance between particle i and j. And r_e is the radius of effect. The models of gradient, divergence and Laplacian are written as

$$\langle \nabla \phi \rangle_i = \frac{D}{n^0}\sum_{j \neq i}\frac{\phi_j + \phi_i}{|r_j - r_i|^2}(r_j - r_i) \cdot W(|r_j - r_i|) \tag{4}$$

$$\langle \nabla \cdot \boldsymbol{V} \rangle_i = \frac{D}{n^0}\sum_{j \neq i}\frac{(\boldsymbol{V}_j - \boldsymbol{V}_i) \cdot (r_j - r_i)}{|r_j - r_i|^2}W(|r_j - r_i|) \tag{5}$$

$$\langle \nabla^2 \phi \rangle_i = \frac{2D}{n^0\lambda}\sum_{j \neq i}(\phi_j - \phi_i) \cdot W(|r_j - r_i|) \tag{6}$$

$$\lambda = \frac{\sum_{j \neq i}W(|r_j - r_i|)|r_j - r_i|^2}{\sum_{j \neq i}W(|r_j - r_i|)} \tag{7}$$

where D is the dimension number, r is the position vector, n^0 is the initial density of particle number and defined as

$$\langle n \rangle_i = \sum_{j \neq i}W(|r_j - r_i|) \tag{8}$$

The pressure fields are obtained through solving the PPE which can be written as below (Lee et al. 2011)

$$\langle \nabla^2 P^{k+1} \rangle_i = (1 - \gamma)\frac{\rho}{\Delta t}\nabla \cdot \boldsymbol{V}_i^* - \gamma\frac{\rho}{\Delta t^2}\frac{<n^k>_i - n^0}{n^0} \tag{9}$$

where Δt is the calculation time step, k and $k+1$ indicate the k th and $k+1$ th time steps, γ is the weight of the particle number density term and is assigned to be 0.01 in present simulations.

particle i before collision   particle j before collision
particle i at the collision moment   particle j at the collision moment
particle i after collision   particle j after collision
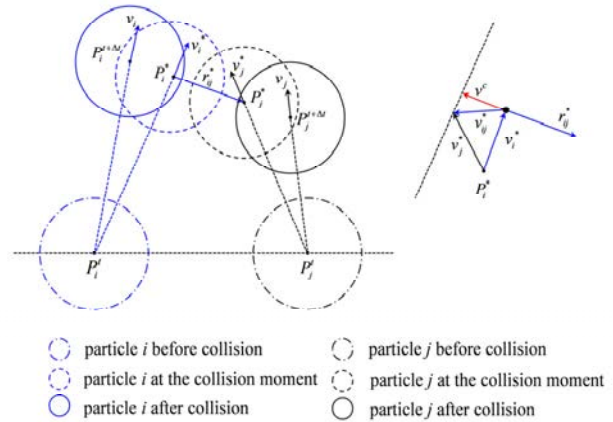
Fig. 1 Schematic diagram of particle interaction model

Particle interaction model

In the calculation of fluid domain, the particles may get very close to each other, resulting in immense repulsive forces between particles. This so-called cluster of particles may lead to non-physical pressure fluctuations and affect the accuracy of calculation. To avoid this

phenomenon, the particle interaction model takes effect when the distance between particles gets smaller than αl_0. l_0 denotes the initial particle spacing and α is the coefficient equals to 0.6 in this paper. The interaction model is depicted in Fig. 1. After the ordinary calculation of MPS, particle j moves from P_j^t to temporary position P_j^* while particle i moves from P_i^t to temporary position P_i^*. If the distance between P_i^* and P_j^* is less than αl_0, a corrective velocity should be imposed on particle i and j to modify their positions. The corrective velocities of particle i and j could be calculated according to Eq. 10.

$$\begin{cases} v_{ij}^* = v_j^* - v_i^* \\ v^c = \dfrac{|v_{ij}^* \cdot r_{ij}^*|}{|r_{ij}^*|} r_{ij}^* \\ v_i = v_i^* + v^c/2 \\ v_j = v_j^* - v^c/2 \end{cases} \tag{10}$$

FEM formulas

The motion of the structural nodes is governed by the following dynamical equation

$$\mathbf{M}\,\ddot{y} + \mathbf{C}\,\dot{y} + \mathbf{K}\,y = \mathbf{F}(t) \tag{11}$$

$$\mathbf{C} = \alpha_1 \mathbf{M} + \alpha_2 \mathbf{K} \tag{12}$$

where $\mathbf{M}$, $\mathbf{C}$ and $\mathbf{K}$ are separately the mass matrix, the Rayleigh damping matrix and the stiffness matrix. $\mathbf{F}$ is the external force vector on nodes and y is the displacement vector of nodes. α_1 and α_2 are coefficients associated with the natural frequency and damping ratio of the structure.

The structural nodal displacement at $t=t+\Delta t$ can be solved with the help of Taylor's expansions of velocity and displacement

$$\dot{y}_{t+\Delta t} = \dot{y}_t + (1-\gamma)\ddot{y}_t \Delta t + \gamma \ddot{y}_{t+\Delta t}\Delta t,\; 0 < \gamma < 1 \tag{13}$$

$$y_{t+\Delta t} = y_t + \dot{y}_t \Delta t + \frac{1-2\beta}{2}\ddot{y}_t \Delta t^2 + \beta \ddot{y}_{t+\Delta t}\Delta t^2,\; 0 < \beta < 1 \tag{14}$$

where β and γ are important parameters of the Newmark-β method, and selected as $\beta=0.25$, $\gamma=0.5$ for all simulations in present paper. Then the displacement at $t=t+\Delta t$ can be solved by the following formula proposed by Hsiao et al. (1999)

$$\bar{\mathbf{K}}\, y_{t+\Delta t} = \bar{\mathbf{F}}_{t+\Delta t} \tag{15}$$

$$\bar{\mathbf{K}} = \mathbf{K} + a_0\mathbf{M} + a_1\mathbf{C} \tag{16}$$

$$\bar{\mathbf{F}}_{t+\Delta t} = \mathbf{F}_t + \mathbf{M}(a_0 y_t + a_2 \dot{y}_t + a_3 \ddot{y}_t) + \mathbf{C}(a_1 y_t + a_4 \dot{y}_t + a_5 \ddot{y}_t) \tag{17}$$

$$a_0 = \frac{1}{\beta\Delta t^2},\; a_1 = \frac{\gamma}{\beta\Delta t},\; a_2 = \frac{1}{\beta\Delta t},\; a_3 = \frac{1}{2\beta}-1,\; a_4 = \frac{\gamma}{\beta}-1,$$
$$a_5 = \frac{\Delta t}{2}\left(\frac{\gamma}{\beta}-2\right),\; a_6 = \Delta t(1-\gamma),\; a_7 = \gamma\Delta t \tag{18}$$

where $\bar{\mathbf{K}}$ and $\bar{\mathbf{F}}$ denote so-called effective stiffness matrix and effective force vector respectively. Finally, the accelerations and velocities corresponding to the next time step are updated as follows

$$\ddot{y}_{t+\Delta t} = a_0(y_{t+\Delta t} - y_t) - a_2\dot{y}_t - a_3\ddot{y}_t \tag{19}$$

$$\dot{y}_{t+\Delta t} = \dot{y}_t + a_6\ddot{y}_t + a_7\ddot{y}_{t+\Delta t} \tag{20}$$

Coupling strategy on interface

The partitioned coupling between MPS and the FEM method is implemented. Sizes of time step for structure analysis and fluid analysis are Δt_s and Δt_f, respectively. Here, Δt_s is k multiples of Δt_f, where k is an integer. The procedure of interaction can be summarized as below.

(1) The fluid field would be calculated k times based on improved MPS method. To obtain the external force on the element node, pressure on boundary particle should be firstly averaged during Δt_s (or $k\cdot\Delta t_f$), as follows

$$\bar{p}_{n+1} = \frac{1}{k}\sum_{i=1}^{k} p_{n+i} \tag{21}$$

where p_{n+i} is the pressure of the fluid particles on wall boundary at the instant $t + i\Delta t_f$, $\bar{p}_{n+1}$ is the averaged pressure of the fluid particle within Δt_s.

(2) Determine the values of structural nodal position y_t, velocity $\dot{y}_t$ and acceleration $\ddot{y}_t$ based on the results of previous time step.

(3) Calculate the external force vector $\mathbf{F}_{t+\Delta t_s}$ of the structural boundary particles based on pressure of fluid wall boundary particles $\bar{p}_{n+1}$.

(4) Calculate the structural nodal displacements and velocities at next structural time step based on the Newmark-β scheme.

(5) Update the velocity and position of the structural boundary particles at each structural time step and the fluid particles at each fluid time step.
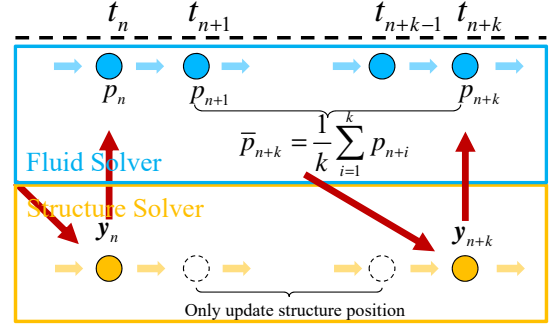
Fig. 2 Data communication strategy on the interface

Numerical wave generation

The solitary wave consists of a single crest with infinite wave length. According to the potential-flow theory, the profile of the solitary wave can be expressed as below

$$\eta = H\,\mathrm{sech}^2(k(x-ct)) \tag{22}$$

$$k = \sqrt{3H/4d^3} \tag{23}$$

$$c = \sqrt{g(H+d)} \tag{24}$$

where H is the wave height, d is the water depth, x is the horizontal coordinate, c is the wave speed, g is the acceleration of gravity, t is the time. In the simulation, the solitary wave is generated through the piston-type wavemaker. The method of wave generation adopted here refers to the research of Goring (1976). The speed of wavemaker is given by the formula below

$$U(t) = \frac{cH\,\mathrm{sech}^2(k(X-ct))}{d + H\,\mathrm{sech}^2(k(X-ct))} \tag{25}$$

Thus the position of wavemaker at time t can be expressed as

$$X(t) = \frac{H}{kd}\tanh(k(ct-X)) \tag{26}$$

The stroke length is calculated by the difference value between the wavemaker position at $t=+\infty$ and $t=-\infty$:

$$S = \sqrt{\frac{16Hd}{3}} \tag{27}$$

The wave period is approximately

$$T \approx \frac{2}{kc}(3.8 + \frac{H}{d}) \qquad (28)$$

After one wave period, the wavemaker reaches its maximum position and then keeps still.

NUMERICAL SIMULATION

Wave impacting onto rigid plate

In this subsection, the problem of wave interacting with a 3D rigid horizontal plate is investigated. The model of the numerical wave tank, as well as the plate, is depicted in Fig. 3. As is shown, the plate is 0.305 m in length, 0.149 m in width and 0.0127 m in thickness. The tank is 2.00 m in length and 0.152 m in width. Compared with the experimental setup, the length of numerical tank is shorten owing to the large requirement of computation amount in MPS method. 701399 particles are used for this simulation. The computer with specifications shown in Table 2 is utilized for present simulation. The adopted time step is 0.0001 s and it takes 496.7 hours to complete the total calculation of 30000 time steps. The calculation of each time step costs 59.6 seconds on average. By the way, the length of physical tank is 7.84 m which require 3302654 particles totally for simulation if the genuine length of experiment is adopted. According to the calculation of only 100 time steps, the time consumed for the calculation of one time step is 431.7 seconds on average. For the simulation of 4 physical seconds, if the time step is set to be 0.0001 s, the approximate calculation time is 4796.7 hours which is unaffordable for us. Actually the issue concerned in this case is the first attack from the solitary wave, which is unlikely to be affected by the subsequent reflection wave. Besides, a wave probe is set at the position of 0.6 m from the wave maker to detect the wave elevation. The wave amplitude for the solitary wave is set to be 0.0343 m according to one case in the experiment. The computational parameters for the MPS method are shown Table 1.

Fig. 3 The scheme of numerical simulation

Fig. 4 shows the wave elevation history of the present numerical simulation and experiment conducted by Seiffert et al. (2014). Two curves display slight differences owing to a wide particle spacing adopted in the simulation. The numerical wave amplitude is slightly larger than that of experimental result. And the water level is elevated after the wave owing to the movement of piston-type wave maker. However, these differences are limited and will not exert a significant influence on the simulation.

Table 1. Computational parameters

Parameter	Value
Water density	1000(kg/m³)
Water depth	0.114(m)
Wave height	0.0343(m)
Kinematic viscosity	1×10⁻⁶(m²/s)
Gravitational acceleration	9.81(m/s²)
Particle spacing	0.0042(m)
Fluid number	448875
Total number	701399

Table 2. Configuration of CPU cluster

Parameters	Values
Processor	Intel Core i7-4790 @ 3.60GHz
Threads	8
Memory	16GB

Fig. 5 shows the comparison of the horizontal and vertical force on the plate between the simulation and experiment. Fig. 6 shows the snapshots at some particular moments. Two figures are considered simultaneously to analyze the interaction procedure. In both numerical and experimental result, it can be observed that the wave first touches plate at 1.63 s and then it takes 0.16 s (at t =1.79s) for vertical force to reach the maximum. It can be inferred from Fig.6(b) that the maximum vertical force corresponds to the moment that wave peak hits the leading edge of plate. In Fig.6(c) we can observe that a high-pressure region around trailing edge sheds downstream. It is reflected in the Fig. 5 that the vertical force drops suddenly. Then the curve reverses and reaches the secondary peak at 1.96 s as the water suffuses the bottom of plate. In the experimental result, however, the curve is much more complicated after the first peak. In the experiment, the vertical force fluctuates mildly after the first peak. It is assumed that the air trapped between the fluid and plate bottom is responsible for this difference. In the research of Khayyer et al. (2016) who investigated the water slamming with both liquid and gas phases considered, it can be easily observed that part of the gas is compressed between the falling plate and surface. And this so-called cushioning effect of air reduces the water-induced impact pressure on the plate. In both numerical and experimental result, the vertical force finally comes to around zero after the solitary wave propagates downstream. In the experiment, the plate is exposed to an evident negative vertical force resulting from the negative pressure while the wave leaving plate. This phenomenon is not evident in simulation. It needs to be noted that the peak value of vertical force in simulation is larger than that in the experiment. After closer inspection, it can partly be explained by the fact that in the experiment there is a tiny clearance (0.015 m) between the lateral side of plate and the wall of

wave tank, through which the fluid would outflow and thus the pressure on the bottom of plate is relieved.

Fig. 7 shows the pressure distribution on the plate bottom. From these pictures, we can have a clear understanding for the wave-plate interaction. A high-pressure region forms after the wave initially touches the leading edge. It spreads downstream and sheds from the trailing edge (see Fig.7(e)~(f)). Then a new high-pressure region, although weaker than the former, emerges at the juncture between wave and plate (see Fig.7(g)). As the wave propagates downstream, the water suffuses the plate bottom (see Fig.7(j)) and produces a uniform pressure distribution. This moment corresponds to the secondary peak in the vertical force history
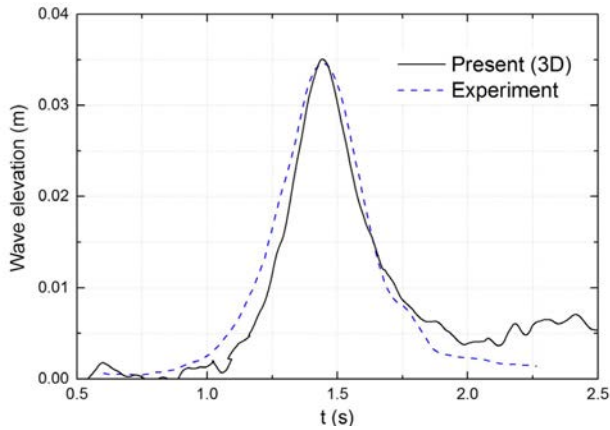
Fig. 4 Wave elevation history in detected point

Wave impacting onto flexible plate

In this subsection, the interaction between solitary wave and flexible plate is investigated through MLParticle-SJTU solver based on the MPS-FEM coupled method. The comparative simulation of wave interacting between the rigid and elastic plate is conducted in 2D. The model for simulation is depicted in Fig. 8. As is shown, the solitary wave is generated with a piston-type wavemaker in a wave tank of 2.50 m in length. A numerical damping domain is set at the end of the tank to avoid the reflection wave. The plate with its size of 0.305 m in length and 0.0127 m in thickness is placed at the position of 0.1254 m above the tank bottom. It is simply supported at each side.

The convergent verification is first conducted to find the appropriate particle spacing for this simulation. The cases of both rigid and flexible plate are considered and the details for the computations are listed in Table 3. The detailed computational parameters for the MPS-FEM coupled method is listed in the Table 4. For the case of rigid plate, the particle spacing (dp) used in verification is 0.0015 m, 0.002 m and 0.0025 m. The corresponding total particle number in the simulation is 134692, 76686 and 43624

respectively. Fig. 9 shows the comparison of wave-induced force history with different particle spacing. The comparisons of the resultant forces between 0.002 m and 0.0015 m show a fair agreement while results of 0.0025 m show an evident distinction. It should be noted that the consumed time for calculation of 0.002 m (4.5 h) is about 37% of the 0.0015 m (12.2 h) under the same hardware condition, as is shown in Table 2.

As for the case of flexible plate, the particle spacing is set to be 0.0015 m (Case 4), 0.002 m (Case 5) and 0.0025 m (Case 6) as well. The corresponding structural element number is 203, 152 and 122 respectively. It should be noted that in present research, the particle spacing for the fluid domain and the element length for the structure domain is identical, which means that the particle and element are refined simultaneously. The comparison of displacement history in the middle of the plate is shown in Fig. 10. The curves of 0.002 m and 0.0015 m show a fair agreement. The obtained wave-induced force history can be seen in Fig. 11. As is shown, the result of 0.0025 m exists marked differences from the other two. Its first peak of vertical force history is evidently higher and there is a discrepancy of phase for the second peak compared with the counterparts of 0.002 m and 0.0015 m. Comparing the resultant force regarding 0.002 m and 0.0015 m, it can be seen that the trends of the two curves are similar. The differences between the two curves might be caused by the complicated interaction between the structural vibration and drastic changes of free surface. And the consumed time for the Case 4~5 is 3.1, 6.8 and 13.3 hours respectively. Judging from the above, the particle spacing of 0.002 m is considered to be efficient in present simulations.

The solitary wave is then generated in numerical tank without plate to verify the accuracy of wave generation. The wave elevation history at monitoring point located 0.6 m far from the wavemaker is given in Fig. 12. Its comparison with experimental result shows a good agreement which indicates that the solver adopted in present paper can generated desired solitary wave in 2D case.

Fig.13 shows the comparison of wave-induced forces between cases of rigid and flexible plate (Case 2 and 5). Evident differences can be observed in the vertical force. For rigid plate, the vertical force reaches maximum at 1.87 s. However, the corresponding peak in the case of flexible plate lags slightly. Fig. 15 can help us clearly observe this distinction: it takes more time for water to suffuse the bottom of flexible plate than that of the rigid plate, or rather the loading duration is longer for the flexible plate. It also results to a slightly lower peak value for flexible plate. Flexible plate possesses a large upward deformation due to the impact, and from Fig.14(c) we can observe that the flexible plate separated from the water which causes a drastic drop in the vertical force. As the deformation maximizes at 2.02 s, the flexible plate starts to move downward and impacts onto the surface at 2.14 s, leading to an impacting force much greater than the first peak. The vertical force returns to steady after a short-time fluctuation. In addition, the comparison of horizontal force between rigid and flexible plate shows a fair agreement.
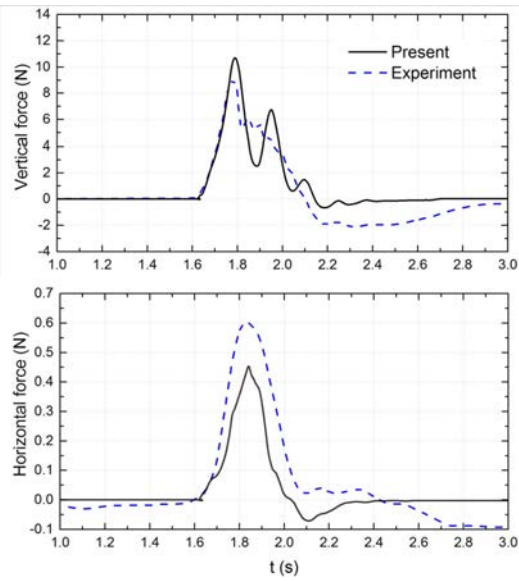
Fig. 5 Comparison of wave-induced forces

(a) t=1.64s   (b) t=1.80s

(c) t=1.82s   (d) t=1.96s

(e) t=2.06s   (f) t=2.20s

Fig. 6 Snapshots of wave-plate interaction

(a) 1.68s (b) 1.72s (c) 1.76s (d) 1.78s

(e) 1.8s (f) 1.82s (g) 1.84s (h) 1.88s

(i) 1.92s (j) 1.96s (k) 2.00s (l) 2.06s
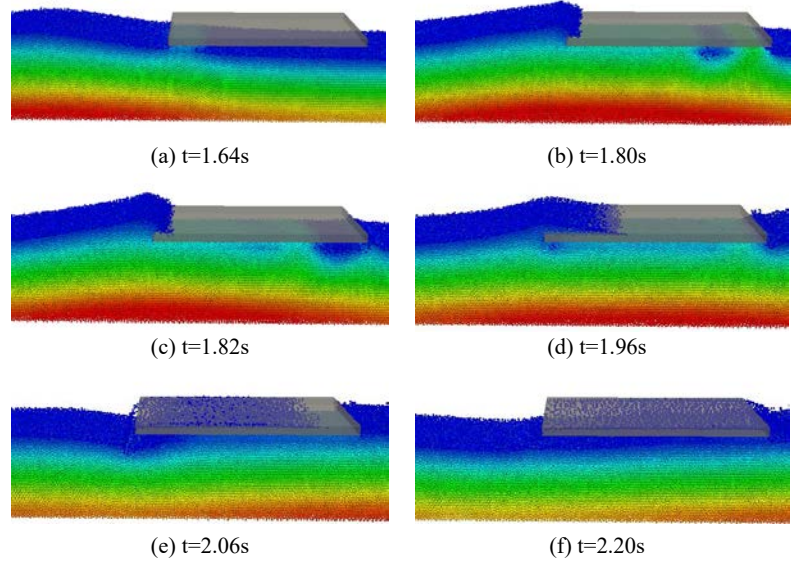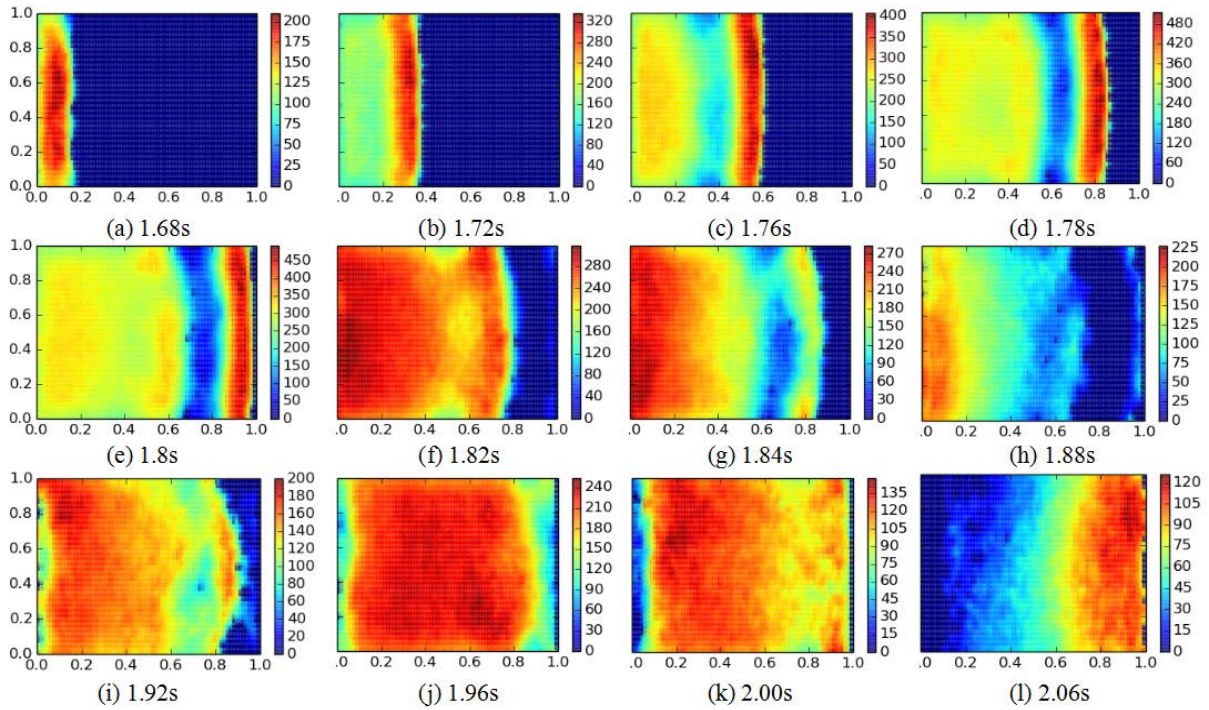
Fig. 7 Pressure distribution on the bottom of plate
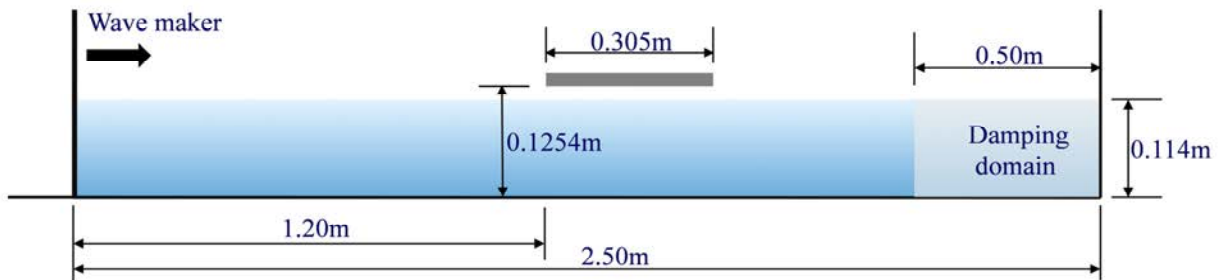
Fig. 8 The scheme of numerical simulation
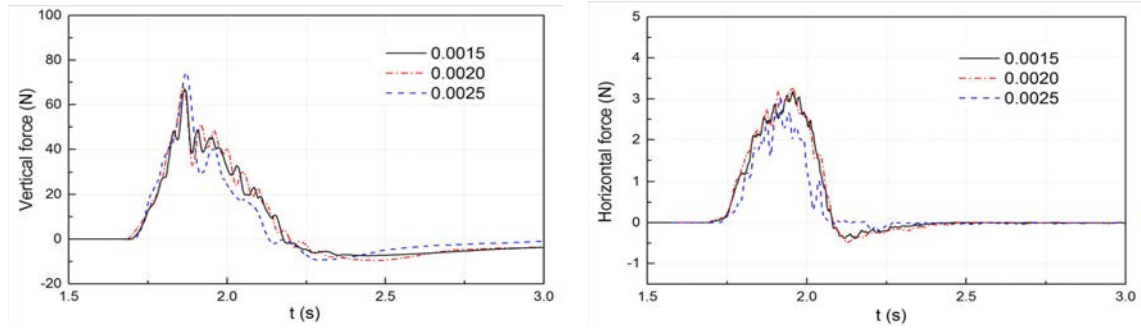
Fig. 9 Comparison of wave-induced force history (For rigid plate)
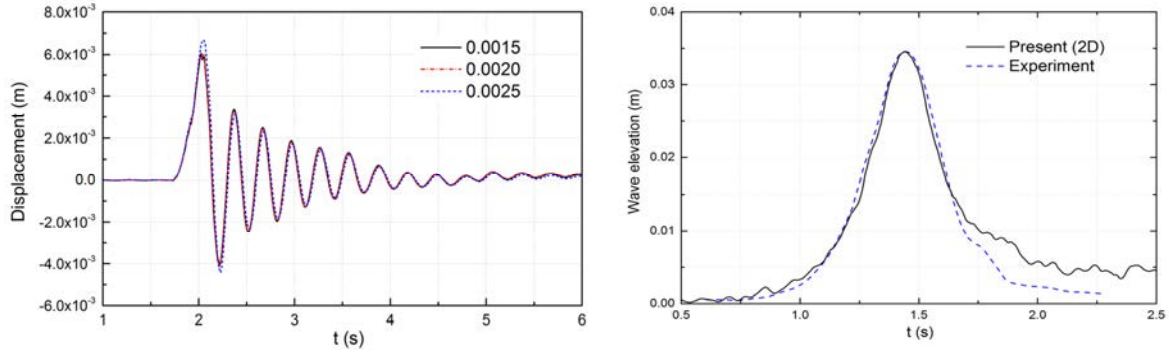
Fig. 10 Comparison of displacement history on the middle of plate

Fig. 12 Wave elevation history in detected point (dp=0.002 m)
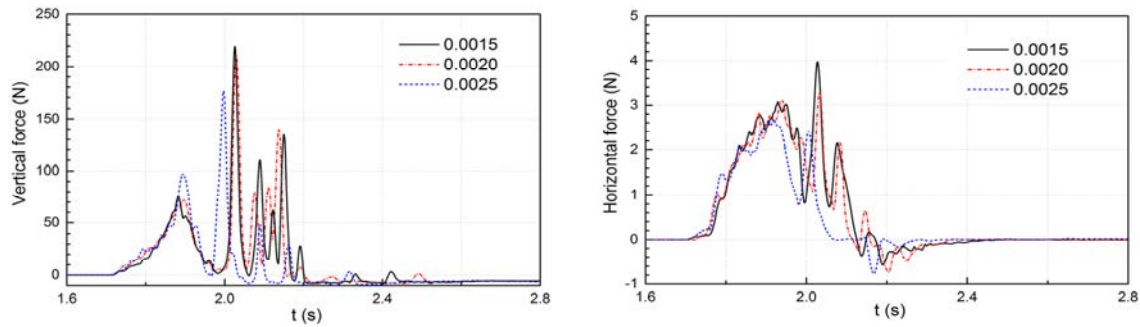
Fig. 11 Comparison of wave-induced force history (For flexible plate)

Table 3. List of all cases

Case	Particle spacing (m)	Element length (m)	Particle number	Element number	Plate
Case1	0.0015	-	134692	-	Rigid
Case2	0.0020	-	76686	-	Rigid
Case3	0.0025	-	43624	-	Rigid
Case4	0.0015	0.0015	133474	203	Flexible
Case5	0.0020	0.0020	76078	152	Flexible
Case6	0.0025	0.0025	43136	122	Flexible

Table 4. Computational parameters

Fluid	Parameters	Values	Structure	Parameters	Values
	Water density	1000(kg/m^3)		Structural density	1040 (kg/m^3)
	Water depth	0.114(m)		Elastic modulus	1(MPa)
	Wave height	0.0343(m)		Cross area	2.5×10^{-5}(m^2)
	Kinematic viscosity	1×10^{-6}(m^2/s)		Inertia moment	1×10^{-3}(m^4)
	Gravitational acceleration	9.81(m/s^2)			
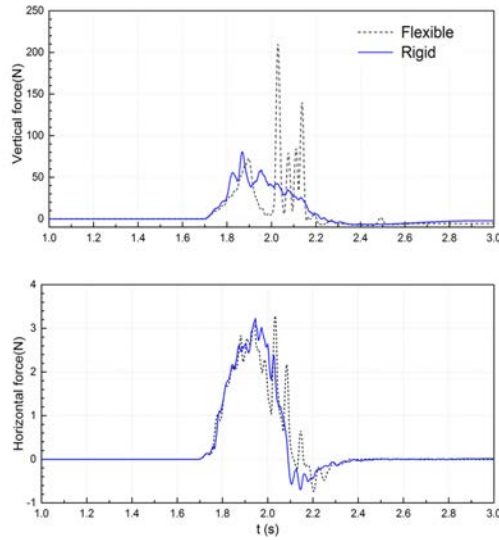
Fig. 13 History of wave-induced forces on plate

(a) t=1.72s   (b) t=1.88s

(c) t=1.94s   (d) t=2.06s

(e) t=2.12s   (f) t=2.20s
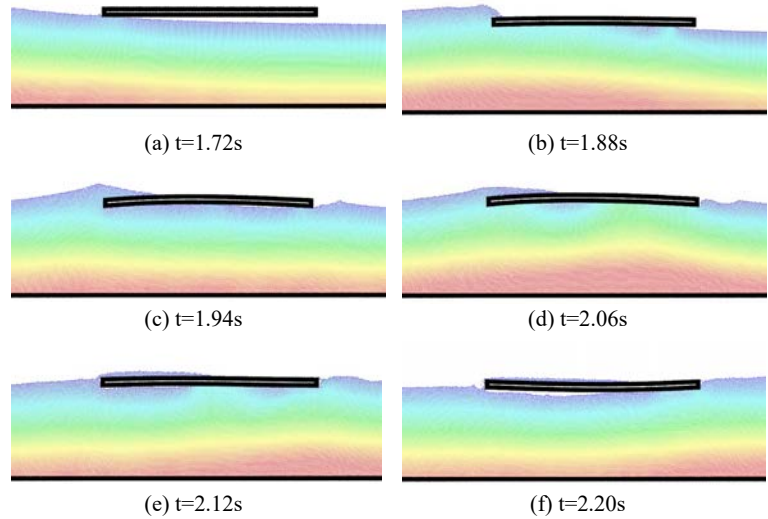
Fig. 14 Snapshots of wave-plate interaction

Plus, the pressure distribution on the bottom of plate with respect to the length is shown in Fig. 16. Results of both the rigid and flexible plate are given in order to investigate the effects of flexibility on wave-induced load. In the early stage of the impact from Fig.16(a) to (d), the pressure distribution forms of the two cases are roughly the same. The effects of flexibility are not obvious as the deformation is still small . As time goes on, however, the effects of flexibility are enhancing - the pressure distribution of flexible case lags behind that of the rigid case gradually and the difference between the maximum of pressure can be observed obviously. The peak pressure happens around 1.84 s for rigid plate while it happens around 1.88 s for the flexible plate whose peak pressure is also 30% less than its counterpart. Then at time of 1.96 s it can be seen that the pressure on the latter part of the flexible plate is dramatically lower than the counterpart. From Fig.14(c), we can see that owing to an upward velocity the bottom of plate separates from the water and leads to a zero-pressure region. This phenomenon corresponds to the drastic drop in the vertical force after the first peak. Subsequently at time around 2.04 s, the flexible plate encounters severe impacting pressure which is much greater than the first peak pressure. It can be inferred from the combination of Fig.10 and Fig.14 that the flexible plate possesses a downward velocity at this moment, causing an intense impact onto the water. This variation is also reflected in the dramatic raise of vertical force around 2.04 s. In the post-impact stage, the pressure on the rigid plate fades gradually, while both the value and distribution of pressure on the flexible plate fluctuates drastically. The pressure distribution is much more concentrative which also indicates the region where the fluid contacts with the flexible plate.

CONCLUSIONS

In present paper, the interaction between the solitary wave and the horizontal flexible plate is numerically investigated. The numerical simulations are conducted through MLParticle-SJTU solver based on MPS-FEM coupled method. The wave-induced force and pressure distribution on the bottom of plate are primarily focused in this research to study the effects of flexibility on wave-plate interaction. Based on the results of numerical simulation, some conclusions are drawn as follows:
a)   In the three-dimensional simulation, the trend of wave-induced force history and the moment at which maximum force occurs agree with the experimental results from Seiffert et al. (2014).

The maximum vertical force happens when the crest of solitary wave hits the leading edge of plate. From the result of pressure distribution, it can be inferred that a high-pressure region emerges at the juncture between wave and plate. As the wave propagates downstream, the high-pressure region sheds from the trailing edge, resulting to a drastic drop in the curve of vertical force. It should be noted that the peak value of wave-induced force is higher than the experimental result. It is because the present calculation ignores the effect of air which can reduce the wave-induced impact pressure on the plate. Thus further research could be focused on creating a two-phase model for MPS method.

b)   In the two-dimensional simulation, the wave-induced forces and pressure distribution on the bottom become more complicated owing to the deformation of the plate. The numerical result shows that it takes more time for water to suffuse the flexible plate above surface than that of the rigid plate. Compared with its counterpart, the first peak of vertical force happens later and is slightly smaller for the flexible plate due to a longer loading time. The pressure distribution on the bottom of plate are also given to analyze the transient loads. It reveals that the evolutions of pressure distribution are similar in the early stage. However, the differences between two cases become evident over time. In the result of flexible plate, an impacting process much severer than the first peak is observed around 2.04 s due to the fact that the plate possesses a downward velocity and thus intensifies its impact with water. Special attention must be paid for this reinforced impacting load.
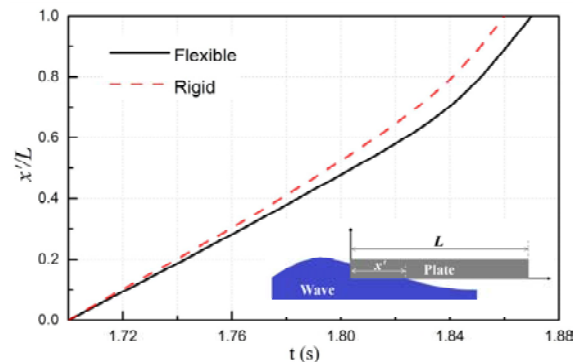
Fig. 15 Time consumed for water to suffuse the bottom
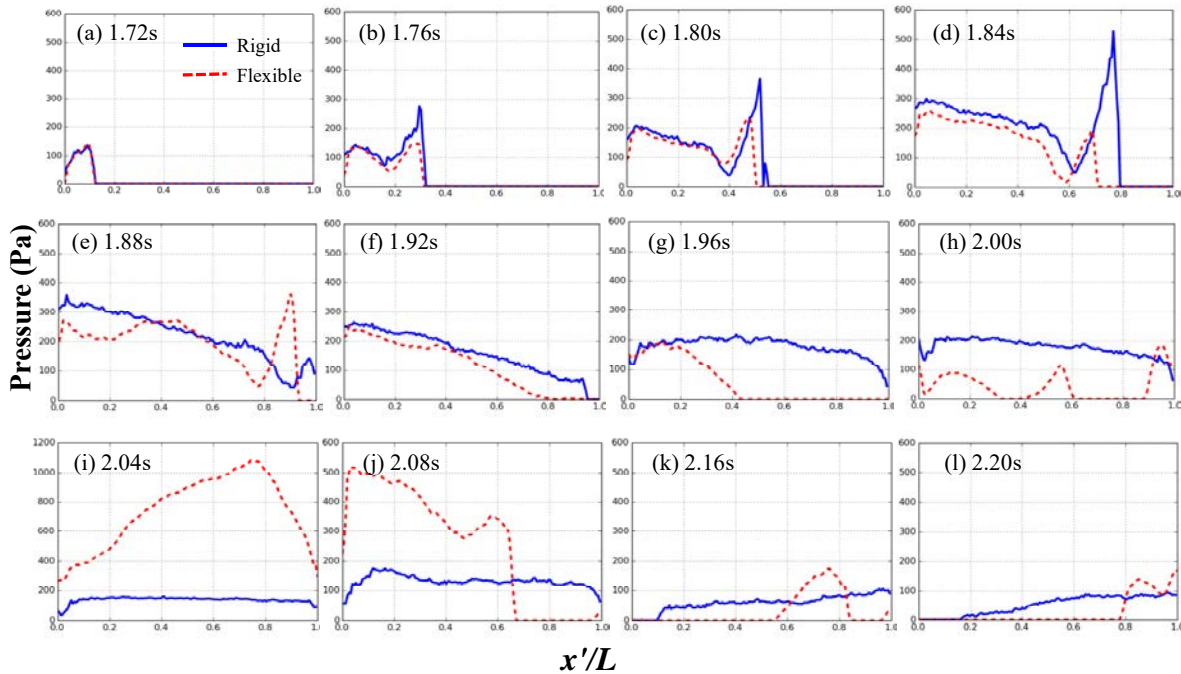
Fig. 16 Pressure distribution on the bottom of plate (Solid: Rigid plate; Dashed: Flexible plate)

REFERENCES

Antoci, C, Gallati, M, and Sibilla, S (2007). "Numerical Simulation of Fluid–structure Interaction by SPH," *Computers and Structures*, 85(11), 879-890.

Attaway, SW, Heinstein, MW, and Swegle, JW (1994). "Coupling of Smooth Particle Hydrodynamics with the Finite Element Method, " *Nuclear engineering and design*, 150(2-3), 199-205.

Allsop, W, Cuomo, G, and Tirindelli, M (2006). "New Prediction Method for Wave-in-deck Loads on Exposed Piers/Jetties/ Bridges," *Coastal Engineering*, 30(5), 4482-4493.

Faltinsen, OM, Kvålsvold, J, and Aarsnes, JV (1997). "Wave Impact on a Horizontal Elastic Plate," *Journal of Marine Science and Technology*, 2(2), 87-100.

Fourey, G, Oger, G, Touzé, DL, and Alessandrini, B (2010). "Violent Fluid-Structure Interaction Simulations using a Coupled SPH/FEM method, " *Iop Conference Series Materials Science & Engineering*, 10, ID.012041.

Goring, DG (1978). "Tsunamis-the Propagation of Long Waves onto a Shelf," Pasadena, California, USA, *California Institute of Technology*.

Gotoh, H, and Khayyer, A (2016). "Current achievements and future perspectives for projection-based particle methods with applications in ocean engineering," *Journal of Ocean Engineering and Marine Energy*, 2(3), 251-278.

Gingold, RA, and Monaghan, JJ (1977). "Smoothed Particle Hydrodynamics: Theory and Application to Non-spherical Stars, " *Monthly notices of the royal astronomical society*, 181(3), 375-389.

Hwang, SC, Khayyer, A, Gotoh, H, and Park, JC (2014). "Development of a Fully Lagrangian MPS-based Coupled Method for Simulation of Fluid-structure Interaction Problems," *Journal of Fluids & Structures*, 50(2), 497-511.

Hwang, SC, Park, JC, Gotoh, H, Khayyer, A, and Kang, KJ (2016). "Numerical Simulations of Sloshing Flows with Elastic Baffles by using a Particle-based Fluid-structure Interaction Analysis Method, " *Ocean Engineering*, 118, 227-241.

Hsiao, KM, Lin, JY, Lin WY (1999). "A Consistent Co-rotational Finite Element Formulation for Geometrically Nonlinear Dynamic Analysis of 3-D Beams, " *Comput. Methods Appl. Mech. Engrg*, 169, 1-18.

Khayyer, A, and Gotoh, H (2016). "A Multiphase Compressible-incompressible Particle Method for Water Slamming," *International Journal of Offshore and Polar Engineering*, ISOPE, 26(01), 20-25.

Khayyer, A, Gotoh, H, and Shimizu, Y (2017). "Comparative study on accuracy and conservation properties of two particle regularization schemes and proposal of an optimized particle shifting scheme in ISPH context," *Journal of Computational Physics*, 332, 236-256.

Kaplan, P, Murray, JJ, and Yu, WC (1995). "Theoretical Analysis of Wave Impact Forces on Platform Deck Structures," *Proc. Int. Conf. on Offshore Mechanics and Arctic Engineering*, ASME, 189-198.

Koshizuka, S, and Oka, Y (1996). "Moving-particle Semi-implicit Method for Fragmentation of Incompressible Fluid," *Nuclear*

science and engineering, 123(3), 421-434.

Lee, BH, Park, JC, Kim, MH, Hwang, SC (2011). "Step-by-step improvement of mps method in simulating violent free-surface motions and impact-loads," *Computer Methods in Applied Mechanics & Engineering*, 200(9-12), 1113-1125.

Lee, CJK, Noguchi, H, and Koshizuka, S (2007). "Fluid–shell Structure Interaction Analysis by Coupled Particle and Finite Element Method, " *Computers and structures*, 85(11), 688-697.

Liao, K, and Hu, C (2013). "A Coupled FDM-FEM Method for Free Surface Flow Interaction with Thin Elastic Plate," *Journal of marine science and technology*, 18(1), 1-11.

Lucy, LB (1977). "A Numerical Approach to the Testing of the Fission Hypothesis, " *The astronomical journal*, 82, 1013-1024.

Lind, SJ, Xu, R, Stansby, PK, and Rogers, BD (2012). "Incompressible Smoothed Particle Hydrodynamics for Free-surface Flows: A Generalised Diffusion-based Algorithm for Stability and Validations for Impulsive Flows and Propagating Waves, " *Journal of Computational Physics*, 231(4), 1499-1523.

Long, T, Hu, D, Yang, G, and Wan, D (2016). "A Particle-element Contact Algorithm Incorporated into the Coupling Methods of FEM-ISPH and FEM-WCSPH for FSI Problems," *Ocean Engineering*, 123, 154-163.

Liu, X, and Sakai, S (2002). "Time Domain Analysis on the Dynamic Response of a Flexible Floating Structure to Waves," *Journal of Engineering Mechanics*, 128(1), 48-56.

Mitsume, N, Yoshimura, S, Murotani, K, and Yamada, T (2014). "Improved MPS-FE Fluid-structure Interaction Coupled Method with MPS Polygon Wall Boundary Model," *Computer Modeling in Engineering & Sciences*, 101(4), 229-247.

Meng, QR, and Lu, DQ (2017). "Wave-induced Hydrodynamic Responses of a Rigid Body Connected with Elastic Plates Floating on a Two-layer Fluid," *Journal of Fluids & Structures*, 68, 295-309.

Nelli, F, Bennetts, LG, Skene, DM, Monty, JP, Lee, JH, Meylan, MH, and Toffoli, A (2016). "Reflection and Transmission of Regular Water Waves by a Thin, Floating Plate," *Wave Motion*, http://dx.doi.org/10.1016/j.wavemoti.2016.08.003

Newmark, NM (1959). "A Method of Computation for Structural Dynamics," *Journal of the engineering mechanics division*, 85(3), 67-94.

Rafiee, A, and Thiagarajan, KP (2009). "An SPH Projection Method for Simulating Fluid-hypoelastic Structure Interaction," *Computer Methods in Applied Mechanics & Engineering*, 198(33-36), 2785-2795.

Seiffert, B, Hayatdavoodi, M, and Ertekin, RC (2014). "Experiments and Computations of Solitary-wave Forces on a Coastal-bridge Deck. Part I: Flat Plate," *Coastal Engineering*, 88, 194-209.

Sun, Z, Djidjeli, K, Xing, JT, and Cheng, F (2016). "Coupled MPS-modal Superposition Method for 2D Nonlinear Fluid-structure Interaction Problems with Free Surface," *Journal of Fluids and Structures*, 61, 295-323.

Tang, ZY, and Wan, DC (2015). "Numerical Simulation of Impinging Jet Flows by Modified MPS Method," *Engineering Computations*, 32 (4), 1153-1171.

Tang, ZY, Zhang, YL, and Wan, DC (2016). "Multi-resolution MPS Method for Free Surface Flows," *International Journal of Computational Methods*, 13 (4), 1641018.

Yang, Q, Jones, V, and McCue, L (2012). "Free-surface Flow Interactions with Deformable Structures using an SPH-FEM Model," *Ocean Engineering*, 55, 136-147.

Zhang, YL., Chen, X, and Wan, DC (2016a). "An MPS-FEM Coupled Method for the Comparative Study of Liquid Sloshing Flows Interacting with Rigid and Elastic Baffles," *Applied Mathematics and Mechanics*, 37(12), 1359-1377. (In Chinese)

Zhang, YL, Tang, ZY, and Wan, DC (2016b). "MPS-FEM Coupled Method for Interaction between Sloshing Flow and Elastic Structure in Rolling Tanks," *Proceedings of the 7th International Conference on Computational Methods*, August 1-4, Berkeley, USA, No. 1493-6106-1-PB.

Zhang, YL, Wan, DC (2017). "Numerical Study of Interactions between Waves and Free Rolling Body by IMPS Method," *Computers and Fluids*, doi: 10.1016/j.compfluid.2017.03.019

Zhang, YX, and Wan, DC (2012). "Apply MPS Method to Simulate Liquid Sloshing in LNG Tank," *Proceedings of 22nd International Offshore and Polar Engineering Conference*, Rhodes, Greece, ISOPE, (3) 381-391.

Zhang, YX, Wan, DC, and Hino, T (2014). "Comparative Study of MPS Method and Level-set Method for Sloshing Flows," *Journal of hydrodynamics*, 26(4), 577-585.